Biology of Reproduction, 2022, **107(2)**,474–487
https://doi.org/10.1093/biolre/ioac078
Advance access publication date 26 April 2022
Research Article

MYO10 promotes transzonal projection-dependent germ line-somatic contact during mammalian folliculogenesis†

Sofia Granados-Aparici[1,2,*], Alexander Volodarsky-Perel[1,2], Qin Yang[2], Sibat Anam[3], Togas Tulandi[1,2], William Buckett[1,2], Weon-Young Son[1], Grace Younes[1,2], Jin-Tae Chung[1], Shaoguang Jin[1], Marie-Emilie Terret[4] and Hugh J. Clarke[1,2,3,*]

[1]Department of Obstetrics and Gynecology, McGill University, Montreal, Canada
[2]Research Institute of the McGill University Health Center, Montreal, Canada
[3]Division of Experimental Medicine, McGill University, Montreal, Canada
[4]Center for Interdisciplinary Research in Biology, Collège de France, CNRS, INSERM, Universitè PSL, Paris, France

*__Correspondence__: Research Institute, McGill University Health Centre, 1001 Boul. Décarie, Montréal, QC H4A 3J1, Canada. Tel: 514-934-1934 x34748; E-mail: sograap@gmail.com or hugh.clarke@mcgill.ca

†__Grant support__: Supported by grants from the Canadian Institutes of Health Research (CIHR; PJT 153122) and the Natural Sciences and Engineering Research Council of Canada (RGPIN-402138) to H.J.C. and the Fonds France Canada pour la Recherche (M.E.T. and H.J.C.). We gratefully acknowledge the generous fellowship support provided by the Réseau Québécois en Reproduction (S.G.A.). H.J.C. holds the Richard Cruess Chair in Reproductive Biology at McGill.

Abstract

Granulosa cells of growing ovarian follicles elaborate filopodia-like structures termed transzonal projections (TZPs) that supply the enclosed oocyte with factors essential for its development. Little is known, however, of the mechanisms underlying the generation of TZPs. We show in mouse and human that filopodia, defined by an actin backbone, emerge from granulosa cells in early stage primary follicles and that actin-rich TZPs become detectable as soon as a space corresponding to the zona pellucida appears. mRNA encoding Myosin10 (MYO10), a motor protein that accumulates at the base and tips of filopodia and has been implicated in their initiation and elongation, is present in granulosa cells and oocytes of growing follicles. MYO10 protein accumulates in foci located mainly between the oocyte and innermost layer of granulosa cells, where it colocalizes with actin. In both mouse and human, the number of MYO10 foci increases as oocytes grow, corresponding to the increase in the number of actin-TZPs. RNAi-mediated depletion of MYO10 in cultured mouse granulosa cell-oocyte complexes is associated with a 52% reduction in the number of MYO10 foci and a 28% reduction in the number of actin-TZPs. Moreover, incubation of cumulus-oocyte complexes in the presence of epidermal growth factor, which triggers a 93% reduction in the number of actin-TZPs, is associated with a 55% reduction in the number of MYO10 foci. These results suggest that granulosa cells possess an ability to elaborate filopodia, which when directed toward the oocyte become actin-TZPs, and that MYO10 increases the efficiency of formation or maintenance of actin-TZPs.

Received: September 23, 2021. **Revised:** February 17, 2022. **Accepted:** April 15, 2022

Graphical Abstract

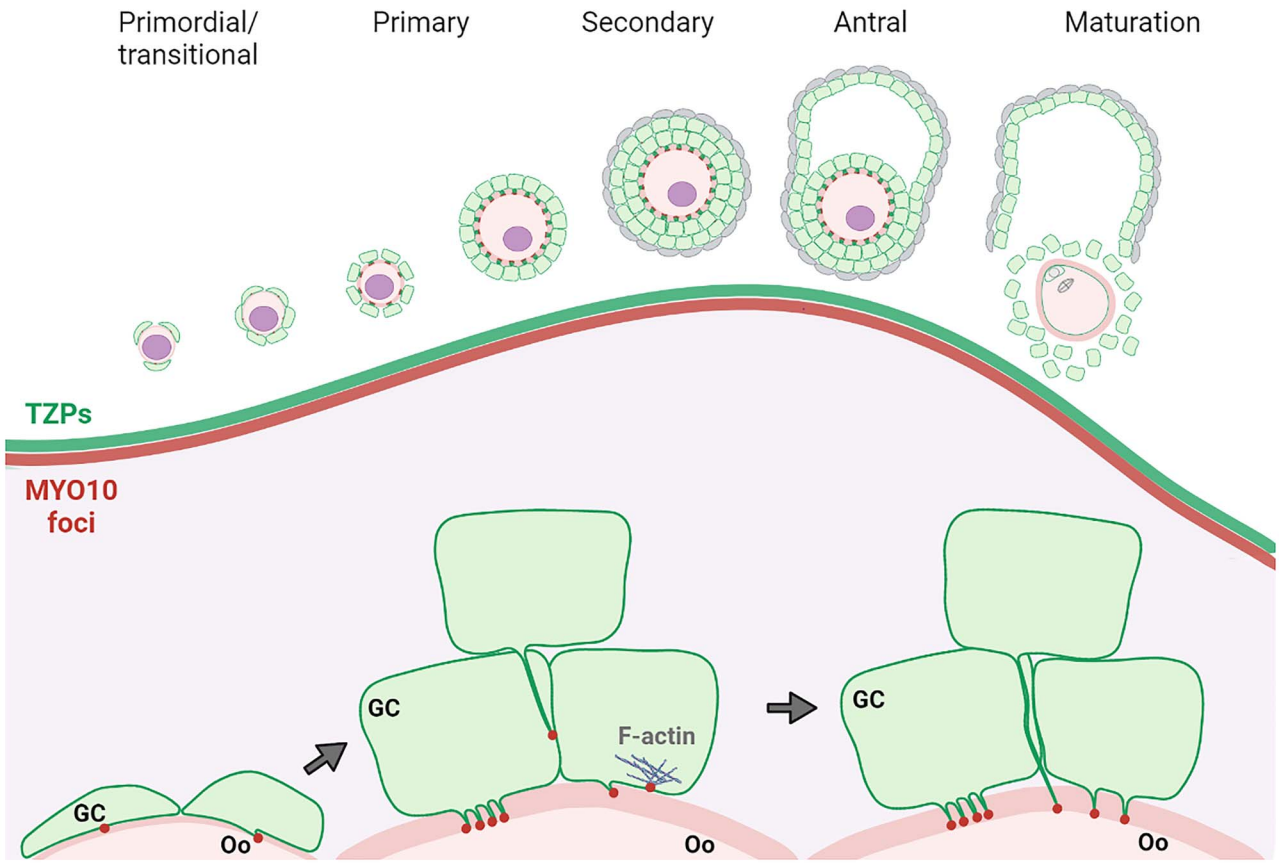

Keywords: oogenesis, folliculogenesis, cell communication, MYO10, filopodia, human infertility

Introduction

Female mammals are born with an ovarian reserve that comprises thousands of small oocytes, each enclosed by a small number of granulosa cells in a primordial follicle [1, 2]. Throughout reproductive life, primordial follicles are regularly activated to enter a prolonged growth phase, during which the oocyte increases in size and the granulosa cells proliferate to generate multiple layers, and which culminates in the production of a developmentally competent egg [3, 4]. During follicular growth, the oocyte and surrounding granulosa cells must remain in physical contact to allow the exchange of essential molecular nutrients and regulatory signals [5]. For example, when granulosa cell-oocyte complexes (GOCs) are isolated from follicles and maintained in vitro, the oocyte will continue to grow if the complex is left intact, but not if it is physically separated from the granulosa cells [6]. Similarly, when gap junctional communication between the two cell types is blocked by mutation of *Gja4*, which encodes connexin37, the oocytes do not grow to full-size and cannot be fertilized [7, 8]. Oocytes and granulosa cells also interact physically via Jagged-Notch binding, where both the ligand and receptor are membrane-associated, although the role of this signaling pathway during growth is not yet fully defined [9].

Within primordial follicles, the granulosa cells lie immediately adjacent to the oocyte, and adherens and gap junctions connect the two cell types [10–13]. After a primordial follicle is activated to begin growth, the oocyte secretes glycoproteins that become assembled into an extracellular matrix known as the zona pellucida [14]. This structure lies between the oocyte and adjacent layer of granulosa cells and physically separates the two cell types. To maintain contact with the oocyte, the granulosa cells elaborate cellular extensions termed transzonal projections (TZPs) that penetrate through the zona pellucida and attach to the oocyte membrane, likely through adherens junctions [13, 15–19]. Two types of TZPs, distinguished by their cytoskeletal backbone, have been identified. One population contains a backbone of F-actin, similar to filopodia, and most studies have focused on these actin-rich TZPs [20–29]. A second population that is present in numerous species including human and nonhuman primates contains a backbone of microtubules [19, 30, 31]. A quantitative analysis in the mouse found that the tubulin-TZPs constitute about 2% of the total population [29]; however, their relative abundance in other species has not been reported. Oocytes of nonmammalian species are also surrounded by an extracellular coat [32], and the somatic follicular cells that lie outside the coat generate TZPs or analogous structures that permit contact and communication with the oocyte [33–35].

Previous studies have shown that as the oocyte and follicle grow, the proliferating granulosa cells generate new actin-TZPs, thereby increasing the total number that contact the oocyte, and experimental studies have confirmed the ability of newly generated actin-TZPs to penetrate the zona pellucida

[16, 20, 36]. Knowledge of when the actin-TZPs first emerge during follicular growth and of what regulates their growth, however, is limited. Scanning electron microscopic images in human revealed that filamentous structures emanate from granulosa cells shortly after activation of follicular growth [11, 37], but did not address their abundance or whether they reached the oocyte. In prepuberal mice lacking growth-differentiation factor 9, a transforming growth factor β family member that is secreted by the oocyte, the number of actin-TZPs is reduced and those that exist are morphologically abnormal [24]. As well, the number of actin-TZPs is decreased in mice that lack proline-rich tyrosine kinase 2, a focal adhesion kinase, in the oocyte [26] or lack the oocyte-specific embryonic poly(A)-binding protein [21]; the latter is associated with reduced E-cadherin in the oocyte. With respect to tubulin-TZPs, gene-knockout and in vitro studies have also shown that follicle-stimulating hormone decreases their number in follicles containing fully grown oocytes [30]. Apart from these data, little mechanistic knowledge exists. Yet this information is important both for understanding how interactions between the oocyte and its environment become established and maintained and for designing and evaluating protocols to support growth of human and animal follicles in vitro.

Myosin 10 (MYO10, also known as Myosin X) plays a key role in the generation of filopodia, which are defined by the presence of an F-actin backbone, in several cell types [38–40]. MYO10 is a member of a family of motor proteins known as myosin tail homology 4-protein 4.1, ezrin, radixin, and moesin myosins, which also contain a motor domain and in the case of MYO10, several pleckstrin homology domains. MYO10 is typically found at the tips of filopodia and has been observed to travel along filopodia [41, 42], suggesting that it transports proteins to the growing tip. MYO10 is also able to initiate filopodial formation [43], and has also been implicated in spindle orientation and function through its ability to bind to microtubules [44–46]. In antral ovarian follicles, large foci of MYO10 are present at the apical (oocyte-facing) surface of granulosa cells in the layer that lies immediately adjacent to oocytes [16]. This strikingly restricted spatial distribution suggests that MYO10 might promote the formation of actin-TZPs similar to its role in the formation of filopodia. Here, we examined the morphology and distribution of actin-TZPs and MYO10 in early growth stage follicles of mouse and human and experimentally evaluated the role of MYO10.

Methods

Mice

All experiments were performed in compliance with the regulations and policies of the Canadian Council on Animal Care and were approved by the Animal Care Committee of the Research Institute of the McGill University Health Centre (RI-MUHC, protocol 7783). CD-1 mice were obtained from Charles River (St-Constant, QC).

Collection and culture of mouse growing GOCs

GOCs were collected as described previously [47, 48]. Briefly, ovaries of 10- to 12-day-old mice were dissected from the ovarian bursa, cut into small fragments, and incubated in HEPES-buffered minimal essential medium (MEM, pH 7.2, Life Technologies, Burlington, ON) containing collagenase (10 μg/ml; Cedarlane, Burlington, ON) and DNase I (10 μg/ml; Sigma) at 37°C in air. Clumps of tissue were aspirated using a micro-tip pipette to disaggregate complexes. Individual GOCs were collected and briefly washed in $NaHCO_3$-buffered MEM. GOCs were transferred to fresh medium and cultured in 4-well plates containing 500 μl of $NaHCO_3$-buffered MEM supplemented with ITS (10 μg/mL insulin, 5.5 μg/mL transferrin and 5 ng/mL selenium; Sigma), FSH (10 mIU/ml; EMD Serono, Mississauga, ON), and estradiol (Sigma, E2758) in an atmosphere of 5% CO_2 in air. For RNAi experiments, Accell *Myo10* siRNA (Dharmacon, GAGGAAGAAUUGUAGAUUAUU and GGAAGAAACUGCAGGGGAUUU) or nontargeting control siRNA (Dharmacon, D-001910-01-05) was added to the culture medium at a final concentration of 1 μM and GOCs were cultured in this solution for 5 days. At the end of culture, GOCs were fixed in freshly prepared 2% paraformaldehyde in phosphate-buffered saline (PBS, pH 7) for 15 min at room temperature or collected for immunoblotting. For immunochemical staining of histological sections, ovaries were placed in 4% paraformaldehyde for 24 h at 4°C and processed in paraffin blocks to obtain 5 μm sections.

Cumulus-oocyte cell complexes (COCs) containing fully grown oocytes were collected from 19- to 21-day-old mice that had received an intraperitoneal injection of 5 IU of equine chorionic gonadotropin (Sigma, Windsor, ON) 44 h previously. To collect COCs and prevent meiotic resumption, antral follicles were mechanically punctured in MEM-H containing cilostamide (20 μM, Sigma). Isolated COCs were directly fixed in freshly prepared 2% paraformaldehyde in PBS (pH 7) for 15 min at room temperature for wholemount staining or allowed to resume meiosis during 8-h culture in cilostamide-free MEM and epidermal growth factor (EGF) (10 ng/ml, BD Biosciences 354 052).

Human ovarian tissue from donors

Ovarian tissue was collected from donors undergoing laparoscopic surgery for benign gynecological disease. All donors gave written informed consent to donate ovarian tissue to the research project. The study was approved by the Research Ethics Board of McGill University Health Centre (MUHC 2018–4004).

Human ovarian tissue preparation and follicle isolation

Fresh ovarian tissue was immediately brought from the operating theatre to the Research Institute for follicle harvesting. The tissue was transferred into fresh HEPES-buffered MEM (pH 7.2, Life Technologies, Burlington, Canada). After excision of damaged and hemorrhagic areas under light microscopy, the tissue was dissected into fragments of $1 \times 1 \times 0.5$ mm^3. Follicle harvesting was performed using modified combined enzymatic and mechanical isolation [49, 50]. The tissue was enzymatically digested by incubation in MEM supplemented with 0.02% DNase (Roche) and 0.28 Wunsch units/mL of Liberase DH (Roche) for 75 min with gentle agitation every 15 min. Neutral red dye at 50 μg/ml (Sigma, N2889) was added to the medium to ensure that viable follicles were retrieved [51]. Neutral red-stained follicles were collected using gentle mechanical isolation with 30-gauge needles and a micropipette and transferred briefly to a dish with culture medium without enzymes. Follicles were

fixed in freshly prepared 2% paraformaldehyde in PBS for 15 min at room temperature.

In situ hybridization

Sections of paraffin-embedded ovaries were deparaffinized using xylene, rehydrated twice with 100% ethanol for 5 min, and air-dried at 60°C in a dry oven for 5 min. Then, slides were processed as indicated by the manufacturer for the RNAscope Multiplex Fluorescent Assay (Advanced Cell Diagnostics, 320850). Briefly, slides were treated with hydrogen peroxide for 10 min at room temperature. Then, slides were rinsed in Milli-Q water and heated in a beaker at 98–100°C for 15 min in 1× target retrieval solution. After rinsing in Milli-Q water for 15 s, slides were transferred in 100% ethanol for 3 min. A hydrophobic barrier was created around the sections using an Immedge pen and slides were incubated with protease solution for 15 min, rinsed in Milli-Q water three to five times, and incubated with Myo10 probe (ACD, 840661) or negative control probe against *Bacillus subtilis DapB* (ACD, 310043) at 40°C for 2 h in a HybEZ oven. Subsequent amplification and detection steps were performed as recommended by the manufacturer and slides were taken for image acquisition using a Zeiss LSM 880 confocal microscope.

Immunoblotting

Granulosa cells from GOCs were isolated by incubation in trypsin–EDTA 0.25% (Thermo Fisher, 25200056) in calcium-free medium (Invitrogen, 21068028) for 10 min at 37°C in air. Trypsin was inactivated with 5% fetal bovine serum and granulosa cells were filtered using a 40-μm Flowmi Cell strainer (Sigma, BAH136800040) to eliminate oocytes. Granulosa cells were then centrifuged at 1500×*g* for 5 min and pellet was lysed in 10 μl of Laemmli buffer. After denaturation at 95°C for 10 min, proteins were separated using precast 12% gels (Bio Rad, 456–8045) and transferred onto a polyvinylidene fluoride membrane (Amersham, Oakville, ON, Canada) under constant voltage. The membrane was subsequently blocked using 5% nonfat milk, in 0.1% Tween-PBS. The membrane was washed three times in Tween-PBS and incubated with primary antibody overnight at 4°C. After washing for 45 min, the membrane was incubated in secondary antibody conjugated to horseradish peroxidase (Promega) at a dilution of 1:5000 for 1 h at room temperature. After washing for 30 min, bound antibody was revealed using ECL+ (Amersham). Antibodies used were anti-MYO10 (Sigma, HPA024223; 1:1000 in PBS containing 0.1% Tween-20 (PBST)) and anti-β-actin (Invitrogen, MA515739; 1:1000 in PBST).

Immunofluorescence staining

Fixed mouse and human follicles were washed three times with PBST and incubated in anti-MYO10 (Sigma, HPA024223; 1:1000 in PBST) in a shaking platform at 4°C overnight. The following day, follicles were washed three times in PBST at room temperature and then incubated for 1 h at room temperature in the Alexa Fluor 555-labeled anti-rabbit IgG (Thermo Fisher, A31572; 1:200 in PBST). F-actin was stained using Alexa Fluor 488-labeled phalloidin (Thermo Fisher, A12379; 1:100 in PBST). DAPI was added to visualize cell nuclei. Follicles were washed twice in PBST for 5 min and then placed in a 2 μl drop of PBS containing 0.3% polyvinylpyrrolidone (Sigma, PVP360) on a glass bottom dish covered with mineral oil. Images were acquired using a Zeiss LSM 880 confocal microscope.

Sections of paraffin-embedded ovaries were deparaffinized using xylene, rehydrated with decreasing ethanol series (100, 90, 70%) for 3 min each, and then placed in Milli-Q water for 5 min. Slides were heated intermittently in a microwave during 20 min in 0.1 M citrate buffer solution at pH 6.0, washed in PBS for 10 min, and blocked with CAS universal blocking solution (Thermo Fisher, 008120) for 30 min at room temperature to reduce nonspecific binding. After overnight incubation with anti-MYO10 antibody, slides were washed three times in PBS at room temperature and then incubated for 1 h at room temperature in the Alexa Fluor 555-labeled anti-rabbit IgG with DAPI. Slides were washed twice in PBS for 5 min and mounted on a drop of VECTASHIELD solution (Vector Laboratories, H-1200-10). Images were acquired using a Zeiss LSM 880 confocal microscope.

Image analysis

Images were obtained as 16-bit RGB stack files. Follicles were imaged with a Plan Apo 63/1.4 oil immersion objective and the following lasers and filters (in parentheses): 488 nm (491–553 nm), 561 nm (571–642) and 405 nm (410–484). Laser strength ranged between 1.5 and 2% and digital gain was adjusted until the first saturated pixels were observed for each channel. A single z-stack image from the cross-section with the largest oocyte diameter and a visible oocyte nucleus was acquired for each follicle. Follicles with a clear resolution of the follicle structures and a visible oocyte nucleus were considered optimal for analysis with Fiji software (National Institutes of Health, Bethesda, MD). Briefly, the region of interest manager tool was used with the composite image to carefully select the area corresponding the granulosa cell area and the zona pellucida.

To quantify the number of F-actin-stained-TZPs (green channel), a segmented circle was drawn around the oocyte in the middle of the zona pellucida, and the fluorescence intensity at each point on the line was obtained. Each point whose value was above the background value of the oocyte cytoplasm and higher than each of its immediately neighboring points was counted as a TZP. For the quantification of MYO10 foci (red channel) in the granulosa cell area, the threshold was adjusted by using the granulosa cell cytoplasm as a baseline setting for negative staining. Only pixels above the threshold were registered as "positive pixels." The resulting positive foci were quantified by using the "Watershed" tool to establish bridges between close foci and the "Analyze particles" tool of particles between >0.2 and 1 μm of diameter (to exclude other bigger aggregations due to saturated pixels in close proximity) allowed the quantification of the MYO10 foci in the selected area. Oocyte diameter (excluding the oocyte cortex and zona pellucida) was measured with the red channel by using the average of two perpendicular lines drawn on the oocyte area. DAPI staining (blue channel) was not thresholded and used to counterstain the granulosa and oocyte.

To determine the relationship between the MYO10 foci and F-actin, Imaris 9.7.2 Software (Bitplane) was used. First, z-stacks of 0.2 μm thickness covering the middle region of a follicle were imaged to obtain a conventional 2D Maximum Intensity Projection (MIP). Then, a 3D rendered surface was created for the F-actin staining with the "Create surface" tool with a surface detail of 0.1 μm and threshold was manually

adjusted based on absolute intensity. A degree of transparency was applied to the created surface to allow visualization of MYO10 foci. To render MYO10 foci, the "Detect Spots" tool was used with an average diameter of 0.3 μm and threshold was manually adjusted based on quality parameters, until all foci from the original image were selected. For visualization purposes, a diameter of 2 μm was used to render MYO10 spots. Once the 3D rendered image with the F-actin surface and MYO10 spots was created, the "Shortest distance of surface to spots" statistical tool was used to obtain the nearest distance from the center of any MYO10 focus to F-actin. A negative value indicated that the MYO10 focus lay within the F-actin border, whereas a positive value indicated that the MYO10 focus lay outside F-actin. In plots of the data, "inside" negative values were displayed in yellow, whereas "outside" positive values were displayed in red.

Follicle stage classification

Primordial follicles contained an oocyte that was enveloped by a single layer of squamous granulosa cells. Transitional follicles contained a mixture of squamous and cuboidal granulosa cells. Primary follicles consisted of a single layer of cuboidal granulosa cells, and multilayered follicles contained several layers of granulosa cells.

Statistical analysis

Data were analyzed and represented using GraphPad Prism 8.4.2 software. Distribution of continuous data was evaluated using the Shapiro–Wilk test. Normally distributed data are presented as mean ± standard error of mean. Statistical significance was evaluated using Student *t*-test with nonparametric Mann–Whitney U test for rank comparison. Pearson correlation test was used for correlation analyses. The *P*-value indicates the probability of obtaining the given data points if the true slope equals zero, which would indicate there is no relationship between the two parameters.

Results

Granulosa cells generate filopodia including actin-TZPs beginning at the primary follicle stage in the mouse

To investigate the pattern and timing of TZP-generation during early folliculogenesis, ovaries of prepubertal female mice were dissociated by mechanical dissection together with mild enzymatic digestion, allowing primordial follicles and granulosa-oocyte complexes (GOCs) from follicles at different stages of growth to be recovered. Fixed follicles and complexes were stained using the F-actin binding protein, phalloidin, and imaged using confocal microscopy. In primordial follicles, which comprise a single layer of squamous granulosa cells surrounding the oocyte, a prominent band of F-actin delineated the cell cortex of both granulosa cells and oocyte (Figure 1A, arrows). In early primary follicles, which contain a single layer of cuboidal granulosa cells with basally positioned nuclei [38], a narrow gap between the granulosa cells and the oocyte was visible in confocal images, representing the region where the zona pellucida is being laid down. Within this region were short actin-rich structures linking the granulosa cells to the oocyte cortex (Figure 1B, arrow). These are by definition TZPs. In more advanced follicles that had begun to generate a second layer of granulosa cells, the actin-TZPs were observed more clearly (Figure 1C, arrow), and filopodia also appeared to be associated with the outer layer of granulosa cells (Figure 1C, arrowhead). Finally, in preantral follicles containing more than two layers of granulosa cells, the actin-TZPs displayed a more perpendicular orientation toward the oocyte plasma membrane (Figure 1D, arrows). These results indicate that a network of actin-TZPs becomes established at or very near the time that the zona pellucida appears during follicular growth in the mouse. They further suggest that filopodia are present on granulosa cells that are not in direct contact with the zona pellucida.

To study the potential role of MYO10 in the formation of actin-TZPs, we first examined its expression in the ovary. RNAscope analysis of paraffin-embedded ovarian sections using a *Myo10* probe revealed a strong signal in follicles (Figure 2A, arrow). Expression was detected in both granulosa cells and oocytes at follicles at all stages of growth (Figure 2B–E). In antral follicles, signal was detected in cumulus granulosa cells surrounding the oocyte and in more distal mural granulosa cells (Figure 2E, arrow). It may be noted also that the signal in the fully grown oocyte was diminished compared with earlier stages. In contrast to the granulosa cells and growing oocytes, only a weak signal was observed in thecal cells or other regions of the ovary. No signal was detected using a control probe (Figure 2F). These observations indicate that within the ovary *Myo10* is expressed at relatively high levels in granulosa cells and growing oocytes.

We then stained and imaged primordial follicles and GOCs using an antibody whose specificity for immunofluorescence has been validated using *Myo10*-knockout mice [39], and which recognizes a prominent band migrating at expected position (~260 kDa) of MYO10 in immunoblots of protein lysates obtained from mid-growth stage follicles (Supplemental Figure S1A). In primordial follicles, foci of staining were observed at the interface between the squamous granulosa cells and the oocyte (Figure 3A, panel I, arrows). In primary follicles, foci were distributed along the circumference of the area between the granulosa cells and oocyte, corresponding to the location of the zona pellucida, and occasionally between granulosa cells (panel II, arrows and arrowhead, respectively). In multilayered and preantral follicles, foci continued to be mainly detected between the innermost granulosa cell layer and the oocyte interface (panels III and IV, arrows). Foci were occasionally observed between granulosa cells within the same or adjacent layers (panels III and IV, arrowheads).

We then stained histological sections of paraffin-embedded ovaries. Similar to the whole-mount specimens, numerous foci of staining were observed in the region between the oocyte and innermost layer of granulosa cells in late primary stage and more advanced follicles (Figure 3B, panels II–IV). Strikingly, however, foci were not observed elsewhere in the follicle nor elsewhere in the tissue sections (panels II–IV). The oocytes of primordial or very early growing follicles were stained (panel I), consistent with the Myo10 mRNA expression pattern described above, but in contrast to the absence of staining in the whole-mount specimens at the same stage (compare Figure 3A, panel I). These results show that foci of MYO10 are present in follicles throughout growth

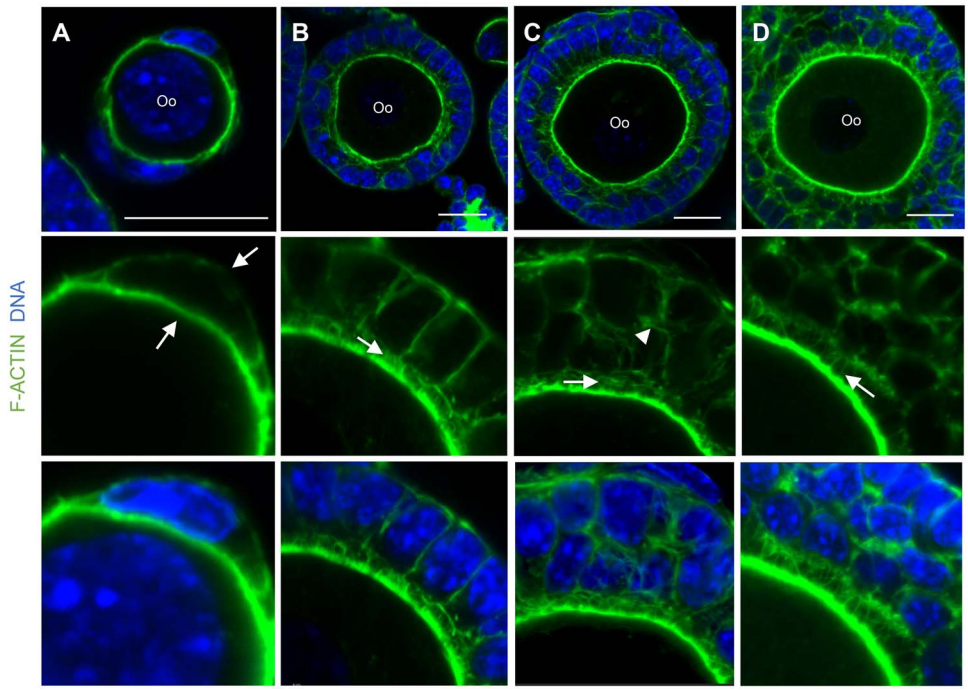

Figure 1. Granulosa cells generate TZPs at early stages of follicle development. Confocal images of isolated mouse follicles stained with phalloidin to stain F-actin (green) and DAPI to stain nuclei (blue). Lower panels show enlarged portions of the corresponding upper panels. (A) Primordial follicle with squamous granulosa cells. Arrows indicate the actin-rich cortex of the oocyte and granulosa cells. (B) Primary follicle containing one layer of cuboidal granulosa cells with basally located nuclei. Arrow indicates TZPs in the space corresponding to the emerging zona pellucida. (C) Multilayered follicle. Arrow and arrowhead indicate TZPs and actin filaments between granulosa cells, respectively. (D) Preantral follicle. Arrow indicates TZPs that are perpendicular to the oocyte plasma membrane. Oo: oocyte. Scale bar = 20 μm.

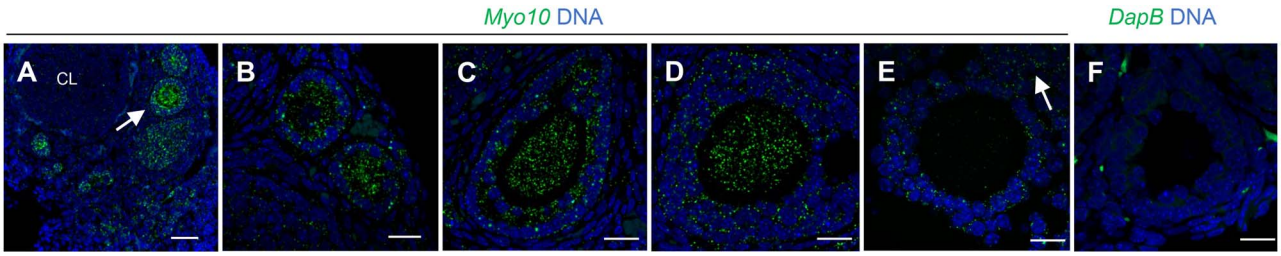

Figure 2. *Myo10* is expressed in the oocyte and granulosa cells in growing follicles. Images of ovarian sections hybridized to probes targeted to *Myo10* or to a control bacterial gene not expressed in mammals. (A) Low-power magnification image shows signal in follicles but not in other cell types including the corpus luteum (CL). (B–D) Higher magnification images of follicles at successively more advanced stages of growth show signal in both granulosa cells and oocyte. (E) Antral follicle shows signal in both cumulus and mural (arrow) granulosa cells, and weaker signal in the oocyte. (F) No signal is detectable using the control probe. Scale bars = 50 μm (A); 20 μm (B–F).

and that they are mainly restricted to the region between the oocyte and innermost granulosa cells.

To quantitatively assess the relationship between the number of MYO10 foci and the stage of follicular development, we counted the number of foci whose diameter was 0.2–1 μm within a region comprising the granulosa cell layers and zona pellucida (Supplemental Figure S1B) in optical sections captured at the maximum oocyte diameter using wholemount GOCs and ovarian sections and plotted this value as a function of oocyte diameter. We observed a positive correlation between the number of foci and oocyte diameter both in isolated GOCs (Figure 3C, Pearson $r = 0.83$; Slope $P < 0.0001$) and in histological sections (Figure 3D, Pearson $r = 0.52$; Slope $P = 0.0002$), although the absolute number of detected foci was lower in the latter compared with the former. These results indicate that the number of MYO10 foci increases as oocytes grow.

MYO10 foci are associated with actin-TZPs in the mouse

We next investigated whether MYO10 was associated with the actin-TZPs. Because TZPs are not detectable using phalloidin in paraffin sections, we examined wholemount preparations. In primordial follicles and early primary follicles containing a single layer of granulosa cells, the MYO10 foci overlapped with F-actin at the cortex of the granulosa cells and at the granulosa cell-oocyte interface (Figure 4A and B, arrows). In more advanced follicles, where the area corresponding to the zona pellucida was clearly evident, MYO10 foci were associated with F-actin including along the shaft of actin-TZPs and at the oocyte cortex (Figure 4C, arrows). The association of MYO10 foci with F-actin between granulosa cells and oocyte and between granulosa cells was also observed in multilayered follicles (Figure 4D, arrow and arrowhead, respectively).

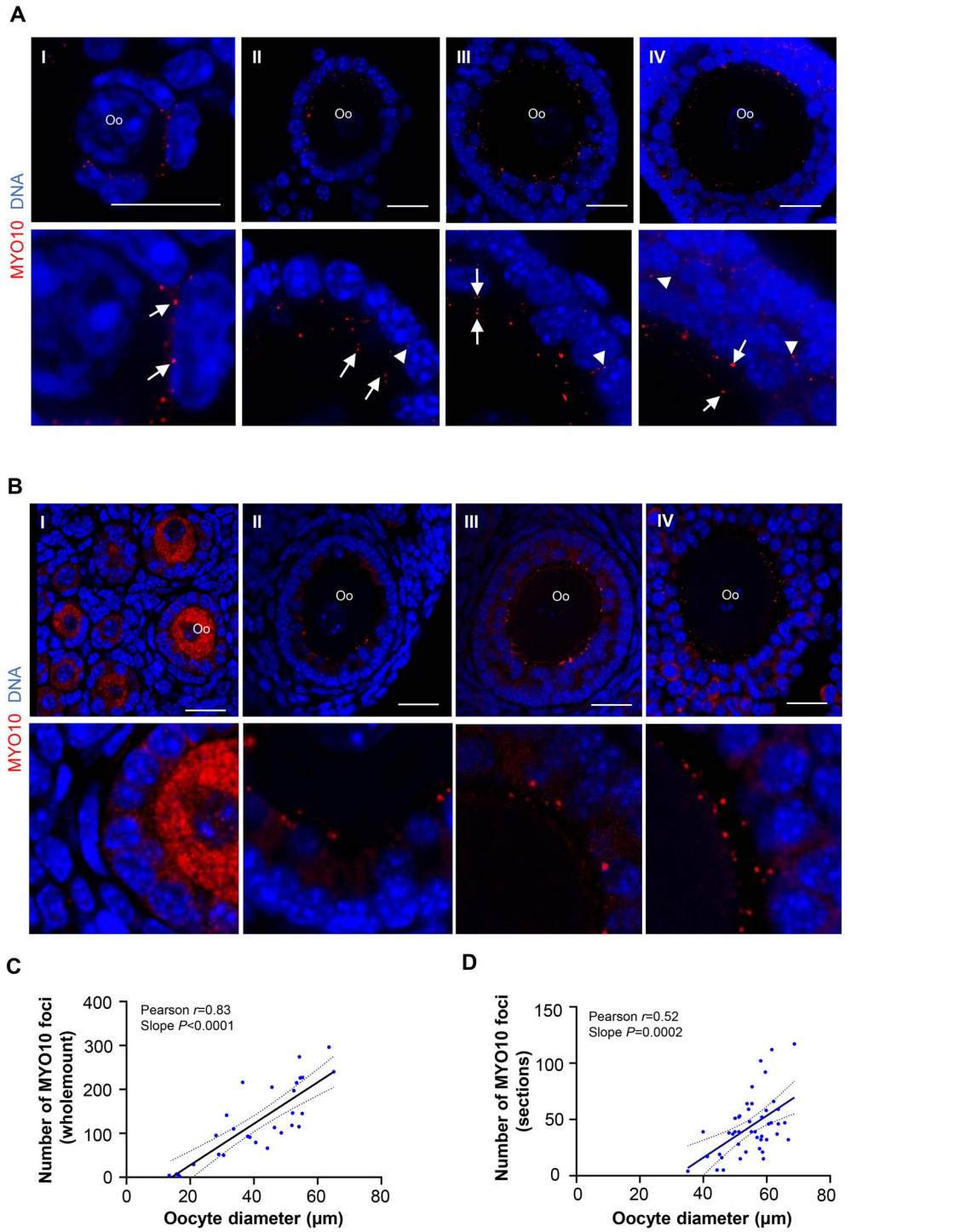

Figure 3. MYO10 foci are found between the granulosa cells and oocyte in growing follicles of the mouse. (A) Confocal images of isolated mouse follicles and granulosa-cell oocyte complexes stained using anti-MYO10 (red) and DAPI (blue). Lower panels show enlarged portions of the corresponding upper panels. Arrows and arrowheads indicate foci of MYO10 between the granulosa cells and oocyte and between granulosa cells, respectively. I. Primordial follicle. II. Single-layer primary follicle. III. Multilayer primary follicle. IV. Preantral follicle. (B) Confocal images of ovarian histological sections stained using anti-MYO10 (red) and DAPI (blue). I. Primordial follicles. II. Single-layer primary follicle. III. Multilayer primary follicle. IV. Preantral follicle. Oo: oocyte. Scale bar = 20 μm. Correlation between the number of MYO10 foci and oocyte diameter in isolated granulosa-oocyte complexes (C) and ovarian sections (D). Statistical analysis using Pearson correlation test. *P*-value indicates the probability that the true value of the slope is zero.

To quantitatively assess the relationship between the MYO10 and F-actin staining, we performed an object-based colocalization analysis to determine the distance between individual MYO10 foci and the nearest region of F-actin. We imaged z-stacks ($n = 30$) spanning 0.2 μm from a single primary follicle to obtain a MIP of F-actin and MYO10 foci. F-actin staining was used to create a 3D surface and MYO10 foci were converted to 3D spots (Supplemental Figure S1C). This allowed us to carry out statistical analyses of volume parameters and calculate the shortest distance of the spots

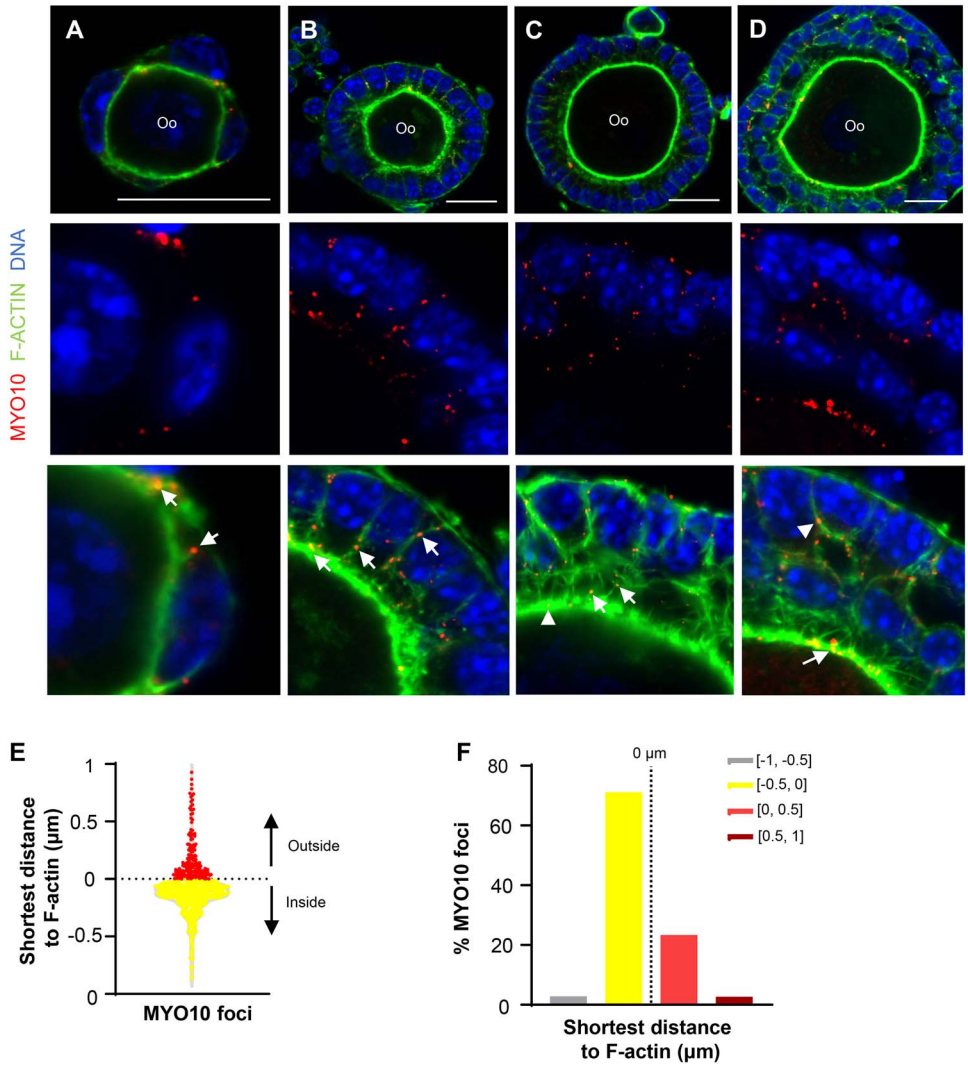

Figure 4. MYO10 foci are associated with TZPs in the mouse. (A–D) Confocal images of isolated mouse follicles and granulosa-cell oocyte complexes stained with phalloidin (green), anti-MYO10 (red) and DAPI (blue). Lower panels show enlarged portions of the corresponding upper panels. Arrows and arrowheads indicate foci of MYO10 between the granulosa cells and the oocyte and between granulosa cells, respectively. (A) Primordial follicle. (B) Single-layer primary follicle. (C) Single-layer primary follicle with zona pellucida present. (D) Multilayer primary follicle. Scale bar = 20 μm. (E) Distribution of foci according to the shortest distance to F-actin. Yellow symbols correspond to foci located within the borders of F-actin (distance <0 μm), red symbols to foci localized outside (distance >0 μm). (F) Proportion of foci located at different distances from the F-actin border.

to surface. About 74% of the MYO10 foci ($n = 745$) were localized within the borders of F-actin (shortest distance to F-actin <0 μm; Figure 4E and F, yellow), whereas 26% were localized outside (shortest distance to F-actin >0 μm, Figure 4E and F, red). Thus, the majority of MYO10 foci are associated with actin-rich structures including TZPs, although a minority are not.

Cytoskeletal dynamics during early human folliculogenesis resemble those of the mouse

We then asked whether these results observed in mouse could be extended to humans. Using tissue that had been donated for research, we investigated the appearance and distribution of actin-TZPs and of MYO10 in human ovarian follicles at early stages of growth. Ovarian fragments were enzymatically digested to isolate individual follicles. Although we were not able to isolate primordial follicles containing only squamous granulosa cells, we obtained transitional follicles that contained a mixture of squamous and cuboidal granulosa cells and primary follicles that contained cuboidal granulosa cells.

As in the mouse, a prominent band of F-actin delineated the cortex of the granulosa cells and the oocyte of transitional follicles (Figure 5A, arrows). In primary follicles containing a single layer of granulosa cells, filopodia could be observed emerging from some of the granulosa cells (Figure 5B, arrows). In larger primary follicles containing a well-defined space between the oocyte and granulosa cells corresponding to the zona pellucida, a network of actin-TZPs was detectable, and these were oriented toward the oocyte (Figure 5C, arrows). In multilayered follicles, the actin-TZP network was dense, and some actin-TZPs appeared to extend from some granulosa cells in distal layers (Figure 5D, arrow). Thus, as in mouse, human granulosa cells generate filopodia, even at early stages of follicular growth, and a dense network of actin-TZPs becomes established as the zona pellucida is laid down.

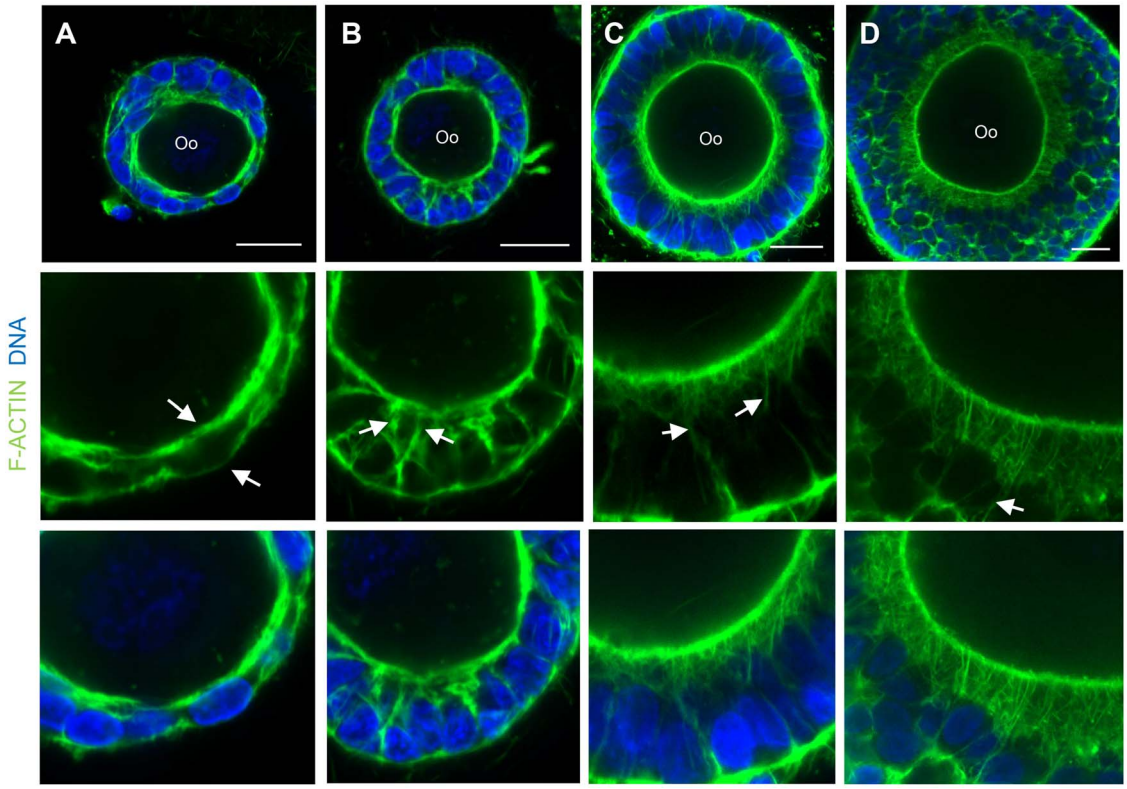

Figure 5. Cytoskeletal dynamics during early human folliculogenesis resemble those of the mouse. Confocal images of isolated human follicles stained with phalloidin (green) and DAPI (blue). Lower panels show enlarged portions of the corresponding upper panels. (A) Transitional follicle. Arrows identify a squamous granulosa cell and oocyte cortex. (B) Primary follicle containing a single layer of granulosa cells. Arrows indicate TZPs emerging from cuboidal granulosa cells. (C) Large primary follicle where zona pellucida fully surrounds the oocyte. Arrows indicate TZPs oriented toward the oocyte. (D) Multilayer follicle. Arrows indicate TZPs emerging from granulosa cells from distal layers. Oo: oocyte. Scale bar = 20 μm.

MYO10 is associated with filopodia and actin-TZPs in humans

Transitional follicles stained using anti-MYO10 antibody displayed a small number of foci that were located at the interface between the granulosa cells and the oocyte and were associated with F-actin (Figure 6A, arrows). In primary follicles at an early stage of growth where no space corresponding to the zona pellucida was yet detectable, F-actin-associated foci were observed between the granulosa cells and the oocyte and also between granulosa cells (Figure 6B, arrow and arrowhead, respectively). The inset in the lower panel shows MYO10 at the tip of an F-actin-based structure emanating from a granulosa cell, strikingly similar to the MYO10 seen at filopodial tips in other cell types [38, 43]. In more advanced follicles containing a space corresponding to the zona pellucida, the foci were more numerous and were mainly localized on the TZPs (Figure 6C and D, arrows). Quantitative analysis of the relationship between the MYO10 foci and F-actin staining revealed that 66% of the MYO10 foci ($n = 74$) were localized within the borders of F-actin (shortest distance to F-actin <0 μm; Figure 6E and F, yellow), whereas 34% were localized outside (shortest distance to F-actin >0 μm, Figure 6E and F, red). Interestingly, there was a positive correlation between oocyte diameter and the number of MYO10 foci (Figure 6G, Pearson $r = 0.30$; $P = 0.013$), as observed in the mouse. These results suggest that MYO10 foci in human ovarian follicles are associated with filopodia including actin-TZPs.

MYO10 promotes establishment or maintenance of actin-TZPs

We then tested whether MYO10 was required for the formation or stability of the actin-TZPs. Because follicles at an early stage of growth contain relatively few actin-TZPs, GOCs obtained from mid-growth stage follicles were incubated in the presence of siRNA targeting *Myo10* or a control (Figure 7A, upper). The siRNA carried a proprietary chemical modification designed to facilitate its incorporation into cells without the use of a lipid-based carrier (see Methods). Following a 5-day incubation, the amount of MYO10 in the granulosa cells was substantially reduced, as detected by immunoblotting (Figure 7B). siRNA-treated GOCs were fixed, stained using anti-MYO10 antibody, and imaged using confocal microscopy. We observed that the number of MYO10 foci in the GOCs that received *Myo10* siRNA was reduced to 0.48 ± 0.05 (mean $\pm$ standard error of the mean) of the control value (Figure 7C, D; $n = 34$ for each group, $P < 0.0001$). We then quantified the number of actin-TZPs in GOCs cultured in the presence of *Myo10* siRNA or control siRNA (see Supplemental Figure S1D). We found that the number of actin-TZPs in the *Myo10* siRNA-treated GOCs was reduced to 0.72 ± 0.06 as compared with the control GOCs (Figure 7C and D; $n = 47$ for control, 44 for experimental; $P = 0.0003$). These results indicate that reducing the amount of MYO10 was associated with a reduction in the number of actin-TZPs.

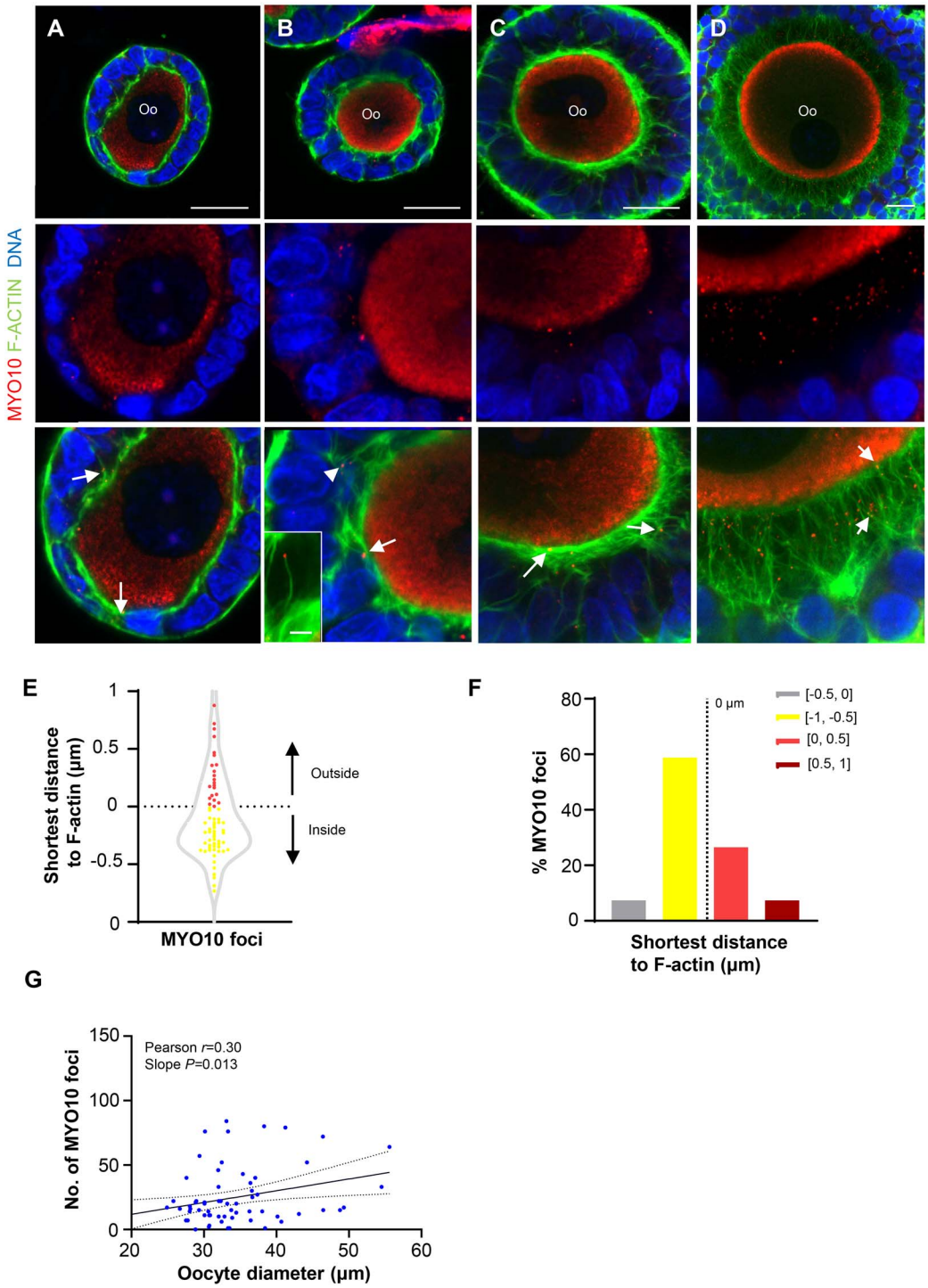

Figure 6. MYO10 is associated with TZPs in humans. (A–D) Confocal images of isolated human follicles stained with phalloidin (green), anti-MYO10 (red), and DAPI (blue). Lower panels show enlarged portions of the corresponding upper panels. Arrows and arrowheads indicate MYO10 foci between the oocyte and granulosa cells and between granulosa cells, respectively. (A) Transitional follicle. (B) Early primary follicle. Inset in bottom panel shows MYO10 at the tip of a filopodium emerging from a granulosa cell. (C) Primary follicle where zona pellucida surrounds the oocyte. (D) Multilayer follicle. Scale bar = 20 μm; bar in inset = 1 μm. (E) Distribution of foci according to the shortest distance to F-actin. Yellow symbols correspond to foci located within the borders of F-actin (distance <0 μm), red symbols to foci localized outside (distance >0 μm). (F) Proportion of foci located at different distances from the F-actin border. (G) Correlation between the number of MYO10 foci and oocyte diameter in follicles. Statistical analysis using Pearson correlation test. *P*-value indicates the probability that the true value of the slope is zero.

We also tested whether, conversely, a reduction in actin-TZPs was associated with a reduction in the number of MYO10 foci. We took advantage of the fact that actin-TZPs undergo a temporally coordinated retraction during meiotic maturation [19, 23, 27, 52]. COCs were obtained from fully grown follicles and either fixed immediately for analysis or were incubated for 8 h in the presence of EGF to induce maturation and then fixed (Figure 7A, lower).

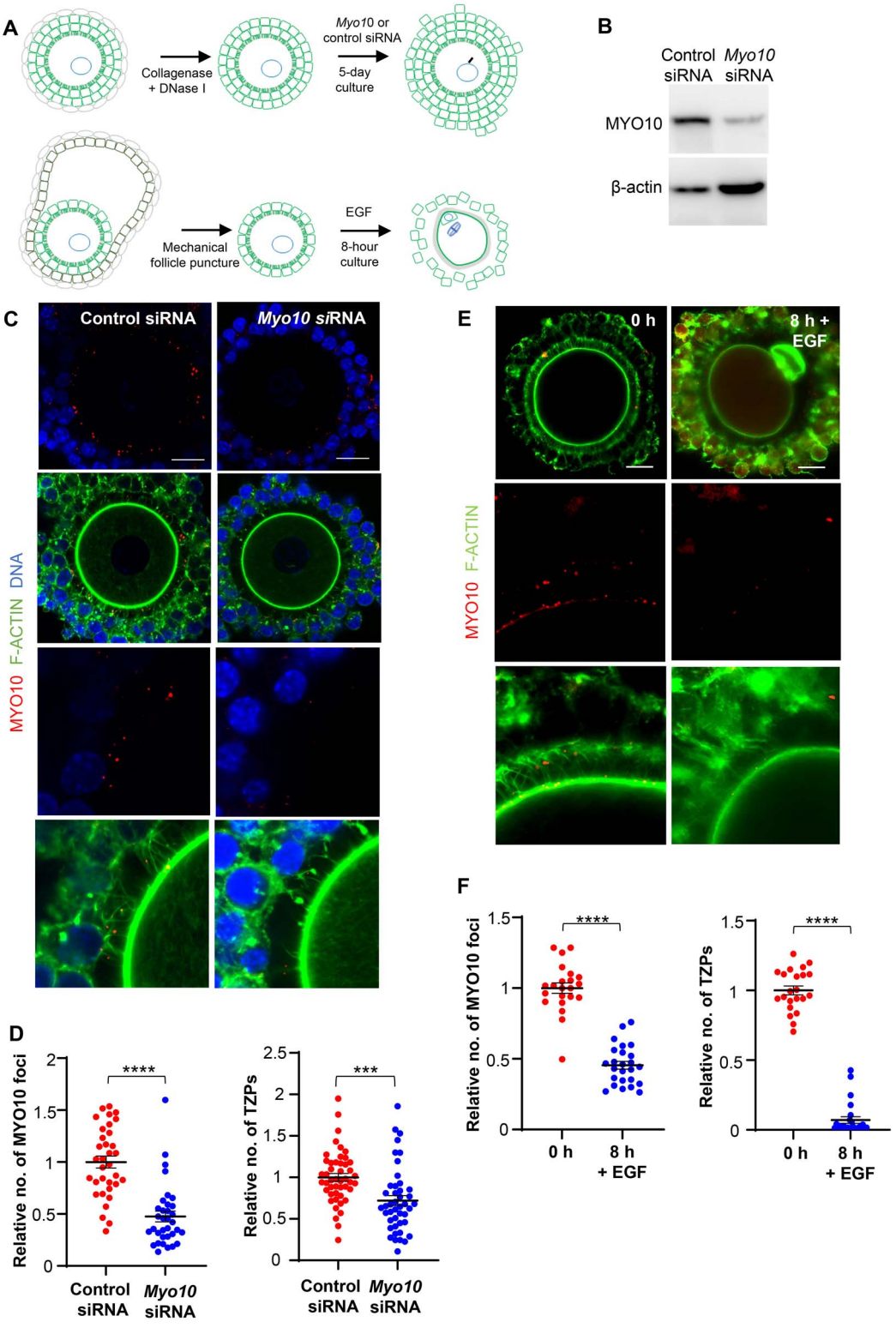

Figure 7. MYO10 is required to establish or maintain TZPs in the mouse. (A) Upper: experimental design for incubating granulosa-oocyte complexes with siRNA targeting *Myo10* or a control. Lower: experimental design for incubating cumulus-oocyte complexes with EGF. (B) Immunoblot showing the amount of MYO10 protein in granulosa cells after siRNA treatment. β-actin used as loading control. (C) Confocal images of siRNA-treated GOCs that were fixed and stained using anti-MYO10 (red), phalloidin (green), and DAPI (blue). Lower panels show enlarged portions of the corresponding upper panels. (D) Number of MYO10 foci (left) and TZPs (right) in GOCs incubated with the indicated siRNAs. (E) Confocal images of siRNA-treated COCs that were fixed immediately after collection (0 h) or treated with EGF for 8 h, stained using anti-MYO10 (red) and phalloidin (green). Lower panels show enlarged portions of the corresponding upper panels. (F) Number of MYO10 foci (left) and TZPs (right) in the two treatment groups. (C, E) Scale bar = 20 μm. (D, F) Mean and SEM values are shown. Statistical analysis using Student t-test. $^{***}P = 0.003$, $^{****}P < 0.0001$.

The COCs were stained using phalloidin and anti-MYO10 antibody, imaged using confocal microscopy, and the number of MYO10 foci and actin-TZPs was quantified as performed for siRNA-treated GOCs. Following the 8-h EGF treatment, the number of actin-TZPs was reduced to 0.07 ± 0.02 (mean ± standard error of the mean) of the number at 0 h (Figure 7E and F; $n = 22$ and $n = 25$ control and matured, respectively, $P < 0.0001$). In the same group of oocytes, the number of MYO10 foci was reduced to 0.45 ± 0.03 (mean ± standard error of the mean) relative to 0 h (Figure 7E and F, $P < 0.0001$). Thus, a decrease in the number of actin-TZPs is associated with a substantial reduction in, though not elimination of, the number of MYO10 foci.

Discussion

TZPs provide the physical basis for the contact between the growing oocyte and the surrounding somatic granulosa cells that is essential to produce a fertilizable egg. We confirm here that actin-TZPs arise and become abundant at the early stages of follicular growth in both mice and humans. TZPs were detectable in transitional and primary follicles—essentially, as soon as a space corresponding to the zona pellucida was apparent between the oocyte and adjacent granulosa cells. We also observed filopodia between granulosa cells of multilayer follicles; the latter being consistent with a previous study of antral follicles which showed that filopodia that do not penetrate the zona pellucida are present on both cumulus and mural granulosa cells [18]. Interestingly, oocytes occasionally develop from primordial germ cells that have migrated to the adrenal medulla; yet, although these oocytes elaborate a zona pellucida, the surrounding somatic cells do not form TZPs [53]. These results suggest that, as previously proposed [18], granulosa cells may possess an inherent ability to elaborate filopodia which when directed toward the oocyte become actin-TZPs.

MYO10 promotes the formation of filopodia, and several lines of evidence reported here support a similar function for MYO10 during the formation or maintenance of actin-TZPs. *Myo10* mRNA was preferentially expressed in the granulosa cells and growing oocytes, as compared with other cell types in the ovary. MYO10 protein accumulated in foci that were detected in the area between the oocyte and innermost layer of granulosa cells, and occasionally between granulosa cells of inner layers, but not in outer layers of granulosa cells further from the oocyte. Thus, the foci were spatially restricted to the region of the TZPs. Moreover, the number of MYO10 foci increased during oocyte and follicular growth, paralleling the increase in the number of actin-TZPs [16]. Experimental depletion of MYO10 from cultured mouse GOCs was associated with a reduction in the number of actin-TZPs, and the natural loss of actin-TZPs during oocyte maturation was accompanied by a reduction on the number of MYO10 foci. On the other hand, mice lacking *Myo10* are fertile, although a detailed examination of their reproductive capacity has not been reported [54, 55]. Taken together, these results suggest that MYO10 increases the efficiency of the formation or maintenance of actin-TZPs.

The specific function of MYO10 with respect to actin-TZPs remains to be established, particularly in view of its multiple roles during filopodial formation [38–40]. Although present throughout the cytoplasm, MYO10 becomes concentrated at the plasma membrane near sites of focal adhesion to the extracellular matrix, where in cooperation with other proteins it promotes the initiation of filopodia, possibly by helping to reorganize F-actin from branched chain to linear filaments [40, 43]. In granulosa cells, the foci of MYO10 near the apical membrane may similarly represent initiation sites. If the specific position of the foci is determined by where the granulosa cell membrane contacts the extracellular matrix (zona pellucida), this would imply a role for the zona pellucida in the initiation of filopodial growth. MYO10 is also located at the tips of growing filopodia [38–40], as we also observed. Here, its activity as an actin-associated motor protein is thought to enable the transport of proteins that favor actin polymerization toward the tip, thereby promoting continued extension of the filopodium [38, 42]. The MYO foci that lie within the zona pellucida and are associated with actin-TZPs may similarly promote their growth. Finally, live-imaging of cells in three-dimensional culture has revealed that MYO10 increases the half-life of filopodia [56], and MYO10 at the tip has also been proposed to interact with cell adhesion molecules, including integrins and cadherins [40, 57–60]. If MYO10 stabilizes growing actin-TZPs, this might increase the probability that they are able to reach the oocyte plasma membrane, and via an interaction with N-cadherin, MYO10 might also promote the attachment of the actin-TZP to the oocyte plasma membrane. Fascin and DAAM1 (disheveled-associated activator of morphogenesis 1), which regulate filopodial growth and morphology [61, 62], are also detectable in actin-TZPs [29], and future work could test the roles of these and other filopodial components in their generation.

Although our results support the idea that many of the MYO10 foci originate from the granulosa cells, *Myo10* mRNA is present in growing oocytes. A previous study showed that fully grown oocytes contain MYO10 and that a MYO10-green fluorescent protein fusion protein expressed in the oocyte becomes localized in foci within the zona pellucida [63]. Recent work has also identified short filopodia that extend from the oocyte into the zona pellucida, although they do not reach the granulosa cells [28]. Intriguingly, we observed MYO10 foci at the tips of short actin projections emanating from the oocyte surface (Supplemental Figure S1E). We speculate that a proportion of the MYO10 foci within the zona pellucida may be located at the tips of the oocyte-derived filopodia.

This study focused on actin-TZPs, so the potential link between MYO10 and tubulin-TZPs remains unknown. It has been proposed that actin-TZPs harbor the gap junctions linking the granulosa cells to the oocyte, whereas tubulin-TZPs harbor the adherens junctions between the two cell types [15], and it is important to experimentally test this conceptually appealing model. In any case, by identifying markers and characteristics of early follicular growth, our results may be relevant to understanding and treating human infertility, particularly in view of recent evidence that impaired interactions with the granulosa cells may play an important role in age-associated loss of fertility [64]. A better understanding of the events and control of early folliculogenesis should aid the development of in vitro systems to favor the production of healthy gametes [65–68].

Acknowledgements

We are grateful to the anonymous donors who provided tissue samples for this research. We thank Drs Shibo Feng and Min Fu (RI-MUHC Imaging Platform) for their invaluable assistance and our colleagues for advice and discussion.

Conflict of Interest Statement

The authors declare no conflicts of interest.

Supplementary material

Supplementary material is available at *BIOLRE* online.

Data availability

All source data will be made available upon reasonable request to the corresponding author.

Author contributions

The project was conceived by S.G.A., A.V.P., and H.J.C. Additional input was provided by M.E.T. Funding was obtained by H.J.C. and M.E.T. Animal experiments were performed by S.G.A., Q.Y., and S.A. Analysis of results was performed by S.G.A. Collection and delivery of clinical samples were organized and overseen by A.V.P. Collection of patient samples was carried out or supervised by T.T., W.B., W.Y.S., G.Y., J.T.C., and S.J. Clinical samples were analyzed by S.G.A. with assistance from A.V.P. The manuscript was written by S.G.A. and edited by S.G.A., M.E.T., and H.J.C.

References

1. Grive KJ, Freiman RN. The developmental origins of the mammalian ovarian reserve. *Development* 2015; **142**:2554–2563.
2. O'Connell JM, Pepling ME. Primordial follicle formation - some assembly required. *Curr Opin Endocr Metab Res* 2021; **18**: 118–127.
3. Zhang H, Liu K. Cellular and molecular regulation of the activation of mammalian primordial follicles: somatic cells initiate follicle activation in adulthood. *Hum Reprod Update* 2015; **21**: 779–786.
4. Sánchez F, Smitz J. Molecular control of oogenesis. *Biochim Biophys Acta* 2012; **1822**:1896–1912.
5. El-Hayek S, Clarke HJ. Control of oocyte growth and development by intercellular communication within the follicular niche. *Results Probl Cell Differ* 2016; **58**:191–224.
6. Eppig JJ. A comparison between oocyte growth in coculture with granulosa cells and oocytes with granulosa cell-oocyte junctional contact maintained in vitro. *J Exp Zool* 1979; **209**: 345–353.
7. Winterhager E, Kidder GM. Gap junction connexins in female reproductive organs: implications for women's reproductive health. *Hum Reprod Update* 2015; **21**:340–352.
8. Simon A, Goodenough D, Li E, Paul D. Female infertility in mice lacking connexin 37. *Nature* 1997; **385**:525–529.
9. Hubbard N, Prasasya RD, Mayo KE. Activation of notch signaling by oocytes and Jag1 in mouse ovarian granulosa cells. *Endocrinology* 2019; **160**:2863–2876.
10. Jorgensen JS. Defining the neighborhoods that escort the oocyte through its early life events and into a functional follicle. *Mol Reprod Dev* 2013; **80**:960–976.
11. Motta P, Makabe S, Naguro T, Correr S. Oocyte follicle cells association during development of human ovarian follicle. A study by high resolution scanning and transmission electron microscopy. *Arch Histol Cytol* 1994; **57**:369–394.
12. Mitchell PA, Burghardt RC. The ontogeny of nexuses (gap junctions) in the ovary of the fetal mouse. *Anat Rec* 1986; **214**: 283–288.
13. Mora JM, Fenwick MA, Castle L, Baithun M, Ryder TA, Mobberley M, Carzaniga R, Franks S, Hardy K. Characterization and significance of adhesion and junction-related proteins in mouse ovarian follicles. *Biol Reprod* 2012; **86**:153.
14. Wassarman PM, Litscher ES. Biogenesis of the mouse egg's extracellular coat, the zona pellucida. *Curr Top Dev Biol* 2013; **102**: 243–266.
15. Li R, Albertini DF. The road to maturation: somatic cell interaction and self-organization of the mammalian oocyte. *Nat Rev Mol Cell Biol* 2013; **14**:141–152.
16. El-Hayek S, Yang Q, Abbassi L, FitzHarris G, Clarke HJ. Mammalian oocytes locally remodel follicular architecture to provide the foundation for germline-soma communication. *Curr Biol* 2018; **28**:1124–1131.
17. Macaulay AD, Gilbert I, Caballero J, Barreto R, Fournier E, Tossou P, Sirard MA, Clarke HJ, Khandjian EW, Richard FJ, Hyttel P, Robert C. The gametic synapse: RNA transfer to the bovine oocyte. *Biol Reprod* 2014; **91**:90.
18. Baena V, Terasaki M. Three-dimensional organization of transzonal projections and other cytoplasmic extensions in the mouse ovarian follicle. *Sci Rep* 2019; **9**:1262.
19. Albertini DF, Rider V. Patterns of intercellular connectivity in the mammalian cumulus-oocyte complex. *Microsc Res Tech* 1994; **27**: 125–133.
20. Herta A-C, Akin N, Billooye K, Saucedo-Cuevas L, Lolicato F, Segers I, Anckaert E, Smitz J. Reversing complete mechanical transzonal projections disruption during mouse in vitro follicle culture with unaltered oocyte competence. *Biol Reprod* 2021; **104**: 1373–1385.
21. Lowther KM, Favero F, Yang CR, Taylor HS, Seli E. Embryonic poly(a)-binding protein is required at the preantral stage of mouse folliculogenesis for oocyte-somatic communication. *Biol Reprod* 2017; **96**:341–351.
22. Macaulay AD, Gilbert I, Scantland S, Fournier E, Ashkar F, Bastien A, Saadi HA, Gagne D, Sirard MA, Khandjian EW, Richard FJ, Hyttel P *et al.* Cumulus cell transcripts transit to the bovine oocyte in preparation for maturation. *Biol Reprod* 2016; **94**: 16.
23. Allworth AE, Albertini DF. Meiotic maturation in cultured bovine oocytes is accompanied by remodeling of the cumulus cell cytoskeleton. *Dev Biol* 1993; **158**:101–112.
24. Carabatsos MJ, Elvin J, Matzuk MM, Albertini DF. Characterization of oocyte and follicle development in growth differentiation factor-9-deficient mice. *Dev Biol* 1998; **204**:373–384.
25. Barrett SL, Shea LD, Woodruff TK. Noninvasive index of cryorecovery and growth potential for human follicles in vitro. *Biol Reprod* 2010; **82**:1180–1189.
26. McGinnis LK, Kinsey WH. Role of focal adhesion kinase in oocyte-follicle communication. *Mol Reprod Dev* 2015; **82**: 90–102.
27. Yuan Y, Spate LD, Redel BK, Tian Y, Zhou J, Prather RS, Roberts RM. Quadrupling efficiency in production of genetically modified pigs through improved oocyte maturation. *Proc Natl Acad Sci U S A* 2017; **114**:E5796–E5804.
28. Zhang Y, Wang Y, Feng X, Zhang S, Xu X, Li L, Niu S, Bo Y, Wang C, Li Z, Xia G, Zhang H. Oocyte-derived microvilli control female fertility by optimizing ovarian follicle selection in mice. *Nat Commun* 2021; **12**:2523.
29. El-Hayek S, Yang Q, Abbassi L, FitzHarris G, Clarke HJ. Mammalian oocytes locally remodel follicular architecture to provide the foundation for germline-soma communication. *Curr Biol* 2018; **28**:1124–1131.
30. Combelles C, Carabatsos M, Kumar T, Matzuk M, Albertini D. Hormonal control of somatic cell oocyte interactions during ovarian follicle development. *Mol Reprod Dev* 2004; **69**: 347–355.

31. Albertini D, Combelles C, Benecchi E, Carabatsos M. Cellular basis for paracrine regulation of ovarian follicle development. *Reproduction* 2001; **121**:647–653.
32. Litscher ES, Wassarman PM. Evolution, structure, and synthesis of vertebrate egg-coat proteins. *Tr Dev Biol* 2014; **8**:65–76.
33. Schroeder TE. Microfilament-mediated surface change in starfish oocytes in response to 1-methyladenine: implications for identifying the pathway and receptor sites for maturation-inducing hormones. *J Cell Biol* 1981; **90**:362–371.
34. Kessel RG, Tung HN, Roberts R, Beams HW. The presence and distribution of gap junctions in the oocyte-follicle cell complex of the zebrafish. *Brachydanio rerio J Submicrosc Cytol* 1985; **17**: 239–253.
35. Browne CL, Werner W. Intercellular junctions between the follicle cells and oocytes of Xenopus laevis. *J Exp Zool* 1984; **230**: 105–113.
36. Fushii M, Yamada R, Lee J, Miyano T. Reestablishment of transzonal projections and growth of bovine oocytes in vitro. *J Reprod Dev* 2021; **67**:300–306.
37. Makabe S, Naguro T, Stallone T. Oocyte-follicle cell interactions during ovarian follicle development, as seen by high resolution scanning and transmission electron microscopy in humans. *Microsc Res Tech* 2006; **69**:436–449.
38. Kerber ML, Cheney RE. Myosin-X: a MyTH-FERM myosin at the tips of filopodia. *J Cell Sci* 2011; **124**:3733–3741.
39. Weck ML, Grega-Larson NE, Tyska MJ. MyTH4-FERM myosins in the assembly and maintenance of actin-based protrusions. *Curr Opin Cell Biol* 2017; **44**:68–78.
40. Houdusse A, Titus MA. The many roles of myosins in filopodia, microvilli and stereocilia. *Curr Biol* 2021; **31**:R586–R602.
41. Kerber ML, Jacobs DT, Campagnola L, Dunn BD, Yin T, Sousa AD, Quintero OA, Cheney RE. A novel form of motility in filopodia revealed by imaging myosin-X at the single-molecule level. *Curr Biol* 2009; **19**:967–973.
42. Berg JS, Cheney RE. Myosin-X is an unconventional myosin that undergoes intrafilopodial motility. *Nat Cell Biol* 2002; **4**: 246–250.
43. He K, Sakai T, Tsukasaki Y, Watanabe TM, Ikebe M. Myosin X is recruited to nascent focal adhesions at the leading edge and induces multi-cycle filopodial elongation. *Sci Rep* 2017; **7**:13685.
44. Kwon M, Bagonis M, Danuser G, Pellman D. Direct microtubule-binding by Myosin-10 orients centrosomes toward retraction fibers and subcortical actin clouds. *Dev Cell* 2015; **34**:323–337.
45. Sandquist JC, Larson ME, Woolner S, Ding Z, Bement WM. An interaction between myosin-10 and the cell cycle regulator Wee1 links spindle dynamics to mitotic progression in epithelia. *J Cell Biol* 2018; 217:849–859.
46. Weber KL, Sokac AM, Berg JS, Cheney RE, Bement WM. A microtubule-binding myosin required for nuclear anchoring and spindle assembly. *Nature* 2004; **431**:325–329.
47. El-Hayek S, Yang Q, Clarke HJ. Growth in vitro of granulosa cell-oocyte complexes of the mouse. *Methods Mol Biol* 2018; **1818**: 1–11.
48. O'Brien MJ, Pendola JK, Eppig JJ. A revised protocol for in vitro development of mouse oocytes from primordial follicles dramatically improves their developmental competence. *Biol Reprod* 2003; **68**:1682–1686.
49. McLaughlin M, Albertini DF, Wallace WHB, Anderson RA, Telfer EE. Metaphase II oocytes from human unilaminar follicles grown in a multi-step culture system. *MHR: Basic Sci Reprod Med* 2018; **24**:135–142.
50. Vanacker J, Camboni A, Dath C, Van Langendonckt A, Dolmans MM, Donnez J, Amorim CA. Enzymatic isolation of human primordial and primary ovarian follicles with Liberase DH: protocol for application in a clinical setting. *Fertil Steril* 2011; **96**: 379–383.e373.
51. Kristensen SG, Liu Q, Mamsen LS, Greve T, Pors SE, Bjørn AB, Ernst E, Macklon KT, Andersen CY. A simple method to quantify follicle survival in cryopreserved human ovarian tissue. *Hum Reprod* 2018; **33**:2276–2284.
52. Abbassi L, El-Hayek S, Carvalho KF, Wang W, Yang Q, Granados-Aparici S, Mondadori R, Bordignon V, Clarke HJ. Epidermal growth factor receptor signaling uncouples germ cells from the somatic follicular compartment at ovulation. *Nat Commun* 2021; **12**:1438.
53. Zamboni L, Upadhyay S. Germ cell differentiation in mouse adrenal glands. *J Exp Zool* 1983; **228**:173–193.
54. Bachg AC, Horsthemke M, Skryabin BV, Klasen T, Nagelmann N, Faber C, Woodham E, Machesky LM, Bachg S, Stange R, Jeong H-W, Adams RH *et al.* Phenotypic analysis of Myo10 knockout (Myo10tm2/tm2) mice lacking full-length (motorized) but not brain-specific headless myosin X. *Sci Rep* 2019; **9**:597.
55. Heimsath EG Jr, Yim YI, Mustapha M, Hammer JA, Cheney RE. Myosin-X knockout is semi-lethal and demonstrates that myosin-X functions in neural tube closure, pigmentation, hyaloid vasculature regression, and filopodia formation. *Sci Rep* 2017; **7**:17354.
56. Summerbell ER, Mouw JK, Bell JSK, Knippler CM, Pedro B, Arnst JL, Khatib TO, Commander R, Barwick BG, Konen J, Dwivedi B, Seby S *et al.* Epigenetically heterogeneous tumor cells direct collective invasion through filopodia-driven fibronectin micropatterning. *Sci Adv* 2020; **6**:eaaz6197.
57. Almagro S, Durmort C, Chervin-Pétinot A, Heyraud S, Dubois M, Lambert O, Maillefaud C, Hewat E, Schaal JP, Huber P, Gulino-Debrac D. The motor protein myosin-X transports VE-cadherin along filopodia to allow the formation of early endothelial cell-cell contacts. *Mol Cell Biol* 2010; **30**:1703–1717.
58. Zhang H, Berg JS, Wang Y, Lång P, Sousa AD, Bhaskar A, Cheney RE, Strömblad S. Myosin-X provides a motor-based link between integrins and the cytoskeleton. *Nat Cell Biol* 2004; **6**: 523–531.
59. Liu KC, Jacobs DT, Dunn BD, Fanning AS, Cheney RE. Myosin-X functions in polarized epithelial cells. *Mol Biol Cell* 2012; **23**: 1675–1687.
60. Lai M, Guo Y, Ma J, Yu H, Zhao D, Fan W, Ju X, Sheikh MA, Malik YS, Xiong W, Guo W, Zhu X. Myosin X regulates neuronal radial migration through interacting with N-cadherin. *Front Cell Neurosci* 2015; **9**:326.
61. Jaiswal R, Breitsprecher D, Collins A, Correa IR Jr, Xu MQ, Goode BL. The formin Daam1 and fascin directly collaborate to promote filopodia formation. *Curr Biol* 2013; **23**:1373–1379.
62. Vignjevic D, Kojima S, Aratyn Y, Danciu O, Svitkina T, Borisy GG. Role of fascin in filopodial protrusion. *J Cell Biol* 2006; **174**: 863–875.
63. Crozet F, Da Silva C, Verlhac MH, Terret ME. Myosin-X is dispensable for spindle morphogenesis and positioning in the mouse oocyte. *Development* 2021; **148**:dev199364.
64. Ben-Meir A, Kim K, McQuaid R, Esfandiari N, Bentov Y, Casper RF, Jurisicova A. Co-enzyme Q10 supplementation rescues cumulus cells dysfunction in a maternal aging model. *Antioxidants (Basel)* 2019; **8**:58.
65. Quan N, Mara JN, Grover AR, Pavone ME, Duncan FE. Spatial analysis of growing follicles in the human ovary to inform tissue engineering strategies. *Tissue Eng Part A* 2020; **26**:733–746.
66. Telfer EE, Zelinski MB. Ovarian follicle culture: advances and challenges for human and nonhuman primates. *Fertil Steril* 2013; **99**:1523–1533.
67. Simon LE, Kumar TR, Duncan FE. In vitro ovarian follicle growth: a comprehensive analysis of key protocol variables†. *Biol Reprod* 2020; **103**:455–470.
68. Gargus ES, Rogers HB, McKinnon KE, Edmonds ME, Woodruff TK. Engineered reproductive tissues. *Nat Biomed Eng* 2020; **4**: 381–393.